Coherent control of the vibrational dynamics of aligned heteronuclear diatomic molecules

László Biró and András Csehi ⬤*

Department of Theoretical Physics, Faculty of Science and Technology,
University of Debrecen, P.O. Box 400, H-4002 Debrecen, Hungary

We present an analytical pulse design protocol for controlling the vibrational dynamics of polar diatomic molecules within a given electronic state. Altering the potential energy function via the position-dependent electric permanent dipole moment, the vibrational state population dynamics is directly controlled using appropriately shaped laser pulses in the midinfrared regime. The optimal pulse shapes—that are expected to drive the molecule along user-defined quantum pathways—are obtained by reverse engineering, that is, solving the Schrödinger equation of the nuclei inversely in a relevant subspace. The proposed control scheme is validated by accurately solving the full time-dependent Schrödinger equation of the HeH$^+$ molecular ion with two completely different methods: (1) propagating the complex population amplitudes of many field-free eigenstates or (2) propagating directly the nuclear wave packet on a grid. We find that besides smooth transitions, arbitrary Rabi oscillations as well as vibrational ladder climbing can be efficiently controlled with the present scheme. As a result, the molecule is successively excited beyond the potential barrier, leading to enhanced dissociation in the ground electronic state. Rotational effects and possible extensions of the presented control are also briefly discussed.

I. INTRODUCTION

The control of atomic and molecular processes using coherent light pulses has gained much interest over the past four decades [1–7]. The ultimate goal of the devised control procedures is designing specific laser pulses to prepare the system under consideration in a desired electronic, vibrational, and rotational state and hence manipulate the outcome of chemical reactions. Several different control strategies have been proposed to selectively guide the system from its initial state to a desired final state with high efficiency. Many of the control scenarios rely on delayed laser pulses. Varying the relative phase or the timing between these control pulses opens up alternative pathways for the system to reach the final target state. By an appropriate tuning of the relative phase or delay parameters, the control of reaction yield or branching ratio of competing channels can be interpreted as the interference of nuclear and/or electronic wave packets [1–3]. Adiabatic passage techniques, like stimulated Raman adiabatic passage (STIRAP), have opened new opportunities for coherent laser control of atomic and molecular processes [4]. To increase the speed of transition, shortcuts to adiabaticity (STA) techniques have been developed [8,9]. Alternative methods, e.g., feedback control [10,11], optimal control [12–18], or reverse engineering [19–24], have been devised, which might be less intuitive but on the other hand very efficient. The laser control of high-dimensional nuclear [25] and coupled nuclear-electronic motion [26–28] has been also addressed based on accurate numerical simulations.

Contrary to weak-field control, where the target states are not altered by the field, a particularly challenging area is the strong-field regime, where the potential energy surfaces (PES) become time-dependent [29–41]. These so-called dynamically Stark shifted (or light-induced) potentials significantly modify the underlying physics and has to be properly taken into account in the control procedure. The dynamic Stark effect (DSE) can be interpreted in the dipole—or in the Raman limit. In the former case the interaction follows the instantaneous electric field, while in the latter one—when the transition is forbidden by symmetry—the interaction follows the laser pulse envelope [30]. It has been shown in recent years that electronically resonant light pulses can give rise to so-called light-induced nonadiabatic phenomena by mixing the electronic and nuclear degrees of freedom of molecules [42–44]. These quantum objects, i.e., conical intersections induced by light, were then found to have significant impact on spectroscopic and dynamical molecular properties in both theory [45–48] and experiment [49–51].

Controlling not only the final state, but also the quantum path completed by the system during the interaction with the laser, is of particular importance [52–58]. In the procedure of reverse engineering, target functions are chosen in advance to define the desired time evolution of the controlled quantities (e.g., state populations and/or phases). After that the Schrödinger equation (or the density equation) is solved inversely to obtain the electric field that drives the system along the prescribed quantum path. In order to find analytical laser pulse shapes, different approximations, e.g., the rotating wave approximation (RWA) [59–63] or adiabatic elimination (AE) [64], are usually applied during the design of the effective few-level model of the atom or molecule

———————
*csehi.andras@science.unideb.hu

under consideration. In some cases the RWA can be avoided, which allows for fast manipulation even in the strong-field regime [22,57].

Two-level systems (TLS) provide a very powerful tool to elucidate complicated light-induced molecular processes. However, in realistic systems the neighboring states can significantly affect the two-level dynamics when the pulse bandwidth is large compared to the relevant detunings. In this case the AE + RWA = AER fails, and as a consequence, a nonnegligible amount of population is distributed on the neighboring states, making the two-level approximation (TLA) inappropriate. One can overcome such difficulties by simply decreasing the pulse bandwidth and compensating the emerging Stark shifts [58] or by exposing constraints to inhibit unwanted transitions [65].

In the present work, we will introduce a pulse design protocol for controlling the internal motion of polar diatomic molecules in a given electronic state. Our scheme to obtain appropriately shaped analytical laser pulses is built on a reverse engineering idea [52], which has been applied in problems like the control of charge migration [53], the control of open systems [54,56], the simultaneous control of population and phase dynamics [55], or strong-field control [57,58]. First, an effective model of the controlled pair of nuclear eigenstates is introduced, which includes the dynamic level shifts caused by the electric permanent dipole moment (PDM) of the molecule. The Schrödinger equation of this model is then solved inversely to find the optimal electric field that drives the molecule along the predefined control function. Besides smooth transitions, Rabi oscillations as well as vibrational ladder climbing [66–75] are efficiently controlled by the present scheme. The presented control may also find application in vibrational quenching, which is a key technique in the formation of ultracold molecules [76]. The validity of the control procedure, which is directly linked to the validity of the RWA and AE, is verified by two different numerical methods: (1) propagating time-dependent expansion coefficients of numerous field-free states (TDEC method) and (2) directly propagating the nuclear wave packet on a grid (TDWP method). For our study, we consider the helium hydride ion (HeH$^+$) as a concrete showcase example, which has been widely studied in recent years [77–83]. Being the simplest polar heteronuclear molecule, HeH$^+$ is an excellent candidate for testing our control scheme. Due to the strong electronic and mass asymmetry, HeH$^+$ has large permanent dipole moment [81]; furthermore as the first excited electronic state has very high energy, single-channel effects dominate, and this molecule behaves analogously to an atom in a laser field [78]. In our analysis, we focus on multistate effects in light of the validity of the RWA and AE; furthermore enhancing the ground-state dissociation of HeH$^+$ is also discussed.

II. MOLECULAR TRANSITIONS

In this section, we describe the theoretical framework of the laser-molecule interaction studied in this work. As a concrete example, we consider the helium hydride molecular ion in the Born-Oppenheimer approximation. Owing to the large separation of the ground and first excited electronic state potentials (>20 eV), the nuclear dynamics of the molecule
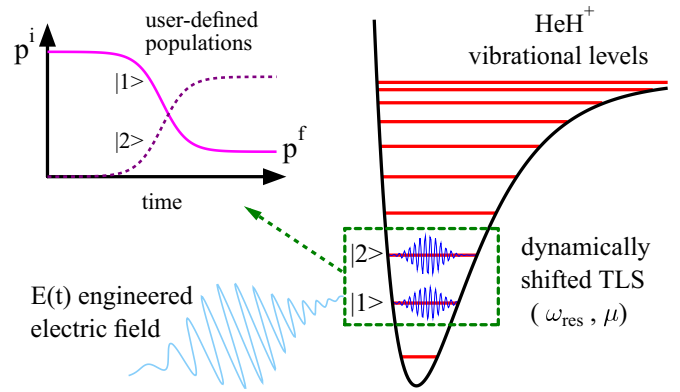
FIG. 1. Schematic representation of the control scenario discussed in this work. The shaped $E(t)$ laser pulse drives the populations of the controlled vibrational states according to a prescribed quantum path. The amplitude and phase of $E(t)$ are engineered such that the dynamical energy level shifts are compensated and the molecule is driven to the desired final quantum state superposition. Controlled Rabi oscillations can be also induced between the states of interest; furthermore an appropriate sequence of different $E(t)$ can induce a vibrational ladder climbing of the molecule. ω_{res} is the resonance angular frequency, and μ is the nuclear transition dipole of the controlled pair of states.

is safely confined to the ground electronic state potential $V_{gr}(R)$ [84] (R is the internuclear distance) for the considered midinfrared (MIR) photon energies. The orientation of the molecular axis is assumed to be parallel with the laser polarization, which allows one to focus on the pure vibrational state control of the system. The molecule is considered initially in the superposition of two of its vibrational eigenstates, e.g., $|1\rangle$ and $|2\rangle$. Applying a coherent laser pulse (to be designed by reverse engineering), the system is transferred to the desired final superposition of the $|1\rangle$ and $|2\rangle$ states along some user-defined control function (see Fig. 1). The field-free molecule is represented by the $H_0 = -\frac{1}{2m_r}\frac{\partial^2}{\partial R^2} + V_{gr}(R)$ nuclear vibrational Hamiltonian and its corresponding $|j\rangle$ eigenstates and ω_j eigenenergies (atomic units are used), where the j index runs over all the vibrational states of the molecule in the ground electronic state (m_r is the reduced mass). The interaction of the molecule with the laser pulse is treated in the dipole approximation, that is, $W(t) = -\vec{d}_{gr} \cdot \vec{E}(t)$, where $\vec{d}_{gr}$ is the R-dependent electric permanent dipole moment vector and $\vec{E}(t)$ is the linearly polarized electric field. Throughout this work, the form of the laser pulse with ω central angular frequency is considered as

$$\vec{E}(t) = \tfrac{1}{2}\varepsilon(t)e^{-i\omega t}\vec{e}_{pol} + \tfrac{1}{2}\varepsilon^*(t)e^{i\omega t}\vec{e}_{pol}, \qquad (1)$$

where $\vec{e}_{pol}$ is the polarization vector, while the $\varepsilon(t)$ complex quantity and its $\varepsilon^*(t)$ complex conjugate include the ε_0 electric field amplitude, the $g(t)$ envelope function and the $\phi(t)$ phase of the field

$$\varepsilon(t) = \varepsilon_0 g(t)e^{i\phi(t)}, \qquad (2a)$$

$$\varepsilon^*(t) = \varepsilon_0 g(t)e^{-i\phi(t)}. \qquad (2b)$$

In the total time-dependent wave function of the system both the bound and continuum states are explicitly included, and it

reads [85]

$$\Psi(t) = \sum_k c_k(t)|k\rangle e^{-i\omega_k t}. \qquad (3)$$

Upon inserting Eq. (3) into the time-dependent Schrödinger equation $i\dot\Psi = [H_0 + W(t)]\Psi$ we arrive at the full set of coupled differential equations for the $c_j(t)$ complex amplitudes,

$$i\dot{c}_j(t) = \sum_k c_k(t) e^{-i\omega_{kj}t} W_{jk}(t), \qquad (4)$$

where $\omega_{kj} = \omega_k - \omega_j$ and the light-matter interaction term is written as $W_{jk}(t) = -E(t)\mu_{jk}$ with $\mu_{jk} = \langle j|d_{\mathrm{gr}}|k\rangle$ being the nuclear permanent dipole ($j = k$) and nuclear transition dipole ($j \neq k$) matrix elements between the corresponding eigenstates of the molecule. Equation (4) is often limited to a relevant subset of the total manifold for practical reasons. To allow for an analytical treatment, two dipole-coupled states of the molecule will be considered among which we aim to control the population dynamics. Denoting these controlled states with labels 1 and 2, Eq. (4) is written as

$$i\begin{pmatrix} \dot{c}_1(t) \\ \dot{c}_2(t) \end{pmatrix} = \begin{pmatrix} -E(t)\mu_{11} & -E(t)\mu e^{-i\omega_{\mathrm{res}}t} \\ -E(t)\mu e^{i\omega_{\mathrm{res}}t} & -E(t)\mu_{22} \end{pmatrix}\begin{pmatrix} c_1(t) \\ c_2(t) \end{pmatrix}, \quad (5)$$

where $\mu = \mu_{12} = \mu_{21}$ is the nuclear transition dipole (assumed real) and $\omega_{\mathrm{res}} = \omega_2 - \omega_1$ is the resonance angular frequency. In case of near-resonant transitions, the off-resonant intermediate states rapidly oscillate and their population during the laser-molecule interaction is negligible. This holds as long as the detunings of these states are large compared to the pulse bandwidth, the one-photon detuning $\delta = \omega - \omega_{\mathrm{res}}$ and the Stark shifts of interest. Making use of the general form of the electric field [Eq. (1)] and applying the RWA, that is dropping terms that oscillate faster than δ, we obtain the following equation:

$$i\begin{pmatrix} \dot{c}_1(t) \\ \dot{c}_2(t) \end{pmatrix} = \begin{pmatrix} S_1(t) & \Omega(t)e^{i(\delta t - \phi(t))} \\ \Omega(t)e^{-i(\delta t - \phi(t))} & S_2(t) \end{pmatrix}\begin{pmatrix} c_1(t) \\ c_2(t) \end{pmatrix}, \qquad (6)$$

where $\Omega(t)$ is the Rabi frequency

$$\Omega(t) = -\tfrac{1}{2}\mu\varepsilon_0 g(t), \qquad (7)$$

and $S_k(t)$ is the dynamic Stark shift of the kth level

$$S_k(t) = -\mu_{kk}E(t). \qquad (8)$$

We note here that $\Omega(t)$ follows the $\varepsilon_0 g(t)$ envelope function of the pulse, while $S_k(t)$ oscillates with the instantaneous value of the electric field.

It is convenient to transform Eq. (6) into the interaction picture for later purposes, according to the well-known formulas $H' = UHU^\dagger + i\hbar\dot{U}U^\dagger$ and $\Psi' = U\Psi$. Applying the unitary transformation matrix (which leaves the populations unchanged)

$$U = \begin{pmatrix} e^{i\int_{-\infty}^t S_1(t')dt'} & 0 \\ 0 & e^{i\int_{-\infty}^t S_2(t')dt'} \end{pmatrix} \qquad (9)$$

the following equation is obtained for the new coefficients:

$$i\begin{pmatrix} \dot{a}_1(t) \\ \dot{a}_2(t) \end{pmatrix} = \begin{pmatrix} 0 & \Omega(t)e^{i\kappa(t)} \\ \Omega(t)e^{-i\kappa(t)} & 0 \end{pmatrix}\begin{pmatrix} a_1(t) \\ a_2(t) \end{pmatrix}, \qquad (10)$$

where the $\kappa(t)$ laser-molecule phase has been introduced using the relative dynamic Stark shift, $\delta S(t) = S_2(t) - S_1(t) = (\mu_{11} - \mu_{22})E(t)$ and its negative integral, $\gamma(t) = -\int_{-\infty}^t \delta S(t')\,dt' = (\mu_{22} - \mu_{11})\int_{-\infty}^t E(t')\,dt'$

$$\kappa(t) = -\int_{-\infty}^t \delta S(t')\,dt' + \delta t - \phi(t). \qquad (11)$$

Modulating the $\phi(t)$ phase of the field such that $\kappa(t)$ remains constant during the light-matter interaction was found a key technique to efficiently transfer electronic state population in strong laser fields [86]. This phase-locking technique is equivalent to maintaining resonance condition at each moment of time during the action of the frequency chirped laser pulse, despite the movement of the energy levels. In contrast to strong-field multiphoton electronic transitions, in the presently investigated molecular transitions, the Stark shifts of the energy levels follow the oscillating electric field via the permanent dipole moments.

In the present work, we aim to derive optimal pulse shapes that compensate the relative dynamic Stark shift and efficiently control the population dynamics between two arbitrary states of the molecule. To do so, we will first predefine the desired evolution pathway of the system and then solve the TDSE [Eq. (10)] inversely for the field. The obtained analytical pulse will be then tested and applied to the HeH$^+$ molecule by solving its TDSE accurately.

III. REVERSE ENGINEERING

Below we discuss the main steps of the proposed reverse engineering method to obtain analytical pulse shapes for control purposes. We start from the Schrödinger equation of the molecule in the two-level approximation [Eq. (10)]. Making use of Eqs. (2a) and (2b), Eq. (7), and Eqs. (10) and (11) can be written as

$$i\dot{a}_1(t) = -\frac{1}{2}\mu\varepsilon^*(t)e^{i\gamma(t)}e^{i\delta t}a_2(t), \qquad (12a)$$

$$i\dot{a}_2(t) = -\frac{1}{2}\mu\varepsilon(t)e^{-i\gamma(t)}e^{-i\delta t}a_1(t). \qquad (12b)$$

These coupled equations for the population coefficients are often propagated in the presence of a given driving field to obtain the time-dependent populations of the system. Here we follow an inverse procedure. First, the desired quantum path of the system is defined, and then Eqs. (12a) and (12b) are solved for the laser pulse that drives the molecule along the prescribed path. Let us express $\varepsilon^*(t)$ from Eq. (12a) and $\varepsilon(t)$ from Eq. (12b) and insert them into the general expression of the pulse in Eq. (1):

$$E(t) = \frac{1}{i\mu}\left[\frac{\dot{a}_2(t)}{a_1(t)}e^{-i\omega_{\mathrm{res}}t}e^{i\gamma(t)} + \frac{\dot{a}_1(t)}{a_2(t)}e^{i\omega_{\mathrm{res}}t}e^{-i\gamma(t)}\right]. \quad (13)$$

The $a_1(t)$ and $a_2(t)$ complex population coefficients are written as

$$a_k(t) = \tilde{a}_k(t)e^{i\varphi_k(t)} \quad (k = 1, 2), \qquad (14)$$

where $\tilde{a}_k(t)$ represent the absolute values and hence are real nonnegative functions. In general, the $\varphi_k(t)$ phases can be time-dependent, which leads to additional frequency chirping

of the pulse, allowing for the control of the phases of the system [55]. As we are interested in the control of the state populations, let us focus on the solution for time-independent phases [52]. Let the population of state $|1\rangle$ evolve according to a continuous function $\eta(t)$, that is $|\tilde{a}_1(t)|^2 = \eta(t)$. Due to the conservation of norm, the population of $|2\rangle$ is then given by $|\tilde{a}_2(t)|^2 = 1 - \eta(t)$. The absolute values of the complex population amplitudes are thus parametrized as

$$\tilde{a}_1(t) = \sqrt{\eta(t)}, \tag{15a}$$

$$\tilde{a}_2(t) = \sqrt{1 - \eta(t)}. \tag{15b}$$

Substituting Eq. (14) into Eq. (13) and making use of Eqs. (15a) and (15b) we have

$$E(t) = \frac{1}{2i\mu} \left[\frac{\dot{\eta}(t)}{\sqrt{\eta(t)(1-\eta(t))}} e^{i[\omega_{res}t + \varphi - \gamma(t)]} \right.$$
$$\left. - \frac{\dot{\eta}(t)}{\sqrt{\eta(t)(1-\eta(t))}} e^{-i[\omega_{res}t + \varphi - \gamma(t)]} \right], \tag{16}$$

where the $\varphi = \varphi_1 - \varphi_2$ relative phase of the controlled states has been introduced. Finally, Eq. (16) can be further written as a real-valued sinusoid function

$$E(t) = \frac{1}{\mu} \frac{\dot{\eta}(t)}{\sqrt{\eta(t)[1-\eta(t)]}} \sin[\omega_{res}t + \varphi - \gamma(t)]. \tag{17}$$

The engineered laser pulse in Eq. (17) is expected to drive the dynamically shifted molecular system along the predefined control function $\eta(t)$. The final form of $E(t)$ is similar to that found recently for controlling electronic transitions [52,55,58] and can be considered a natural extension to molecular vibrational transitions where dynamic Stark shifts—caused by the electric permanent dipole moment—become relevant. Due to the $\gamma(t)$ term, Eq. (17) represents a frequency-modulated laser pulse. It is important to note that $\gamma(t)$ depends on $E(t)$; therefore its actual form can be found in an iterative manner.

Several different shapes can be chosen for $\eta(t)$ in Eq. (17). The most important boundary condition for these control functions is that their time derivative vanish at the beginning and at the end of the control process to ensure the finite duration of $E(t)$. One of the simplest choice for $\eta(t)$ is a function that smoothly connects an arbitrary initial population value $p^i = |a_1(t = -\infty)|^2$ and a desired final one $p^f = |a_1(t = \infty)|^2$:

$$\eta(t) = \frac{p^i e^{-\alpha t} + p^f}{1 + e^{-\alpha t}}. \tag{18}$$

Here the positive α parameter controls the rate of transition in the populations around the center of the pulse ($t = 0$). The above population control function [Eq. (18)] prescribes half a Rabi cycle. In Sec. IV, a more general form of $\eta(t)$ will be also presented to induce several Rabi oscillations between the controlled pair of states of the molecule. Inserting Eq. (18) into Eq. (17), we arrive at the concrete form of $E(t)$ for driving smooth transitions:

$$E(t) = \frac{1}{\mu} \frac{\alpha e^{\alpha t}(p^f - p^i)(e^{\alpha t} + 1)^{-1}}{\sqrt{[p^i + p^f e^{\alpha t}][(1 - p^i) + (1 - p^f)e^{\alpha t}]}}$$
$$\times \sin[\omega_{res}t + \varphi - \gamma(t)]. \tag{19}$$

Applying Eq. (19), the molecule is driven from an arbitrary initial population distribution of two of its vibrational states to a desired final one. The α control parameter allows one to control not only the final state of the system, but the quantum path (hence the speed of transition) that connects the initial and final state vectors. Fast transitions (large α) imply short pulses which may not drive the system precisely along the user-defined path due to the breakdown of the applied approximations (TLA + RWA). This issue will be analyzed in the next section by exactly solving the full TDSE of the molecule.

IV. RESULTS AND DISCUSSION

Let us start by applying the general engineered laser pulse [Eq. (17)] to control an arbitrary vibrational excitation of HeH$^+$. The smooth transition between two controlled states is described by the target function in Eq. (18) with which the actual form of the laser pulse is given in Eq. (19). To be specific, we set the molecule initially in the superposition of the $|1\rangle$ and $|2\rangle$ states with a population ratio 0.3:0.7 and require the final population ratio 0.8:0.2 of these states, respectively. This is equivalent to setting $p^i = 0.3$ and $p^f = 0.8$ in Eq. (19). The remaining control parameters ω_{res} and μ are obtained from the solution of the stationary Schrödinger equation [84] (for the sake of simplicity $\varphi = 0$ is applied throughout the paper). Due to the $\gamma(t)$ term, Eq. (19) represents a single chirped laser pulse with a frequency modulation dictated by the electric field via the permanent dipoles of the controlled states [see around Eq. (11)]. As $\gamma(t)$ does depend on $E(t)$, its shape is determined by iteration. Using the properly converged $\gamma(t)$, the resonance condition is fulfilled by the pulse at each moment of time despite the movement of the molecular levels. The obtained results are depicted in Fig. 2 for different values of the α transition rate parameter. Here two kinds of numerical simulation results are shown: (1) solving Eq. (5) of the two-level model—where the RWA is not applied—carries information on the limits of the RWA and (2) while solving Eq. (4) in the space of many eigenstates (TDEC method [84]) reveals the applicability of the AE and hence the limits of the TLA. As seen in Fig. 2(a), if the desired transition is slow ($\alpha < 10^{-3}$ a.u.), then both kinds of numerical results nicely follow the target values (dashed-dotted horizontal lines). In this case the laser pulse is of moderate intensity, supports many cycles and has a long duration, thus a narrow bandwidth [Fig. 2(b)]. As a result, both the RWA and AE are satisfied, and the molecule perfectly follows the prescribed path [Fig. 2(e)].

As soon as the required speed of transition (and the value of α) is increased, the field gets stronger and shorter [possessing fewer cycles, Fig. 2(c)], and as a consequence the accurate multilevel (TDEC) numerical results start to deviate from the control functions. For $\alpha > 10^{-3}$ a.u., due to the broader pulse bandwidth, the neighboring states ($|0\rangle$ and $|3\rangle$) start to get populated by the field [dotted line in Fig. 2(a)] and the multilevel results do not follow the target functions anymore. This is attributed to the failure of the adiabatic elimination and hence the breakdown of the two-level approximation [light blue shaded area in Fig. 2(a)]. Further increasing α, the TLA populations continue to follow the target values up to $\alpha \sim 10^{-2}$ a.u. because there are no other available states in the two-level description. Beyond $\alpha \sim 10^{-2}$ a.u. when the
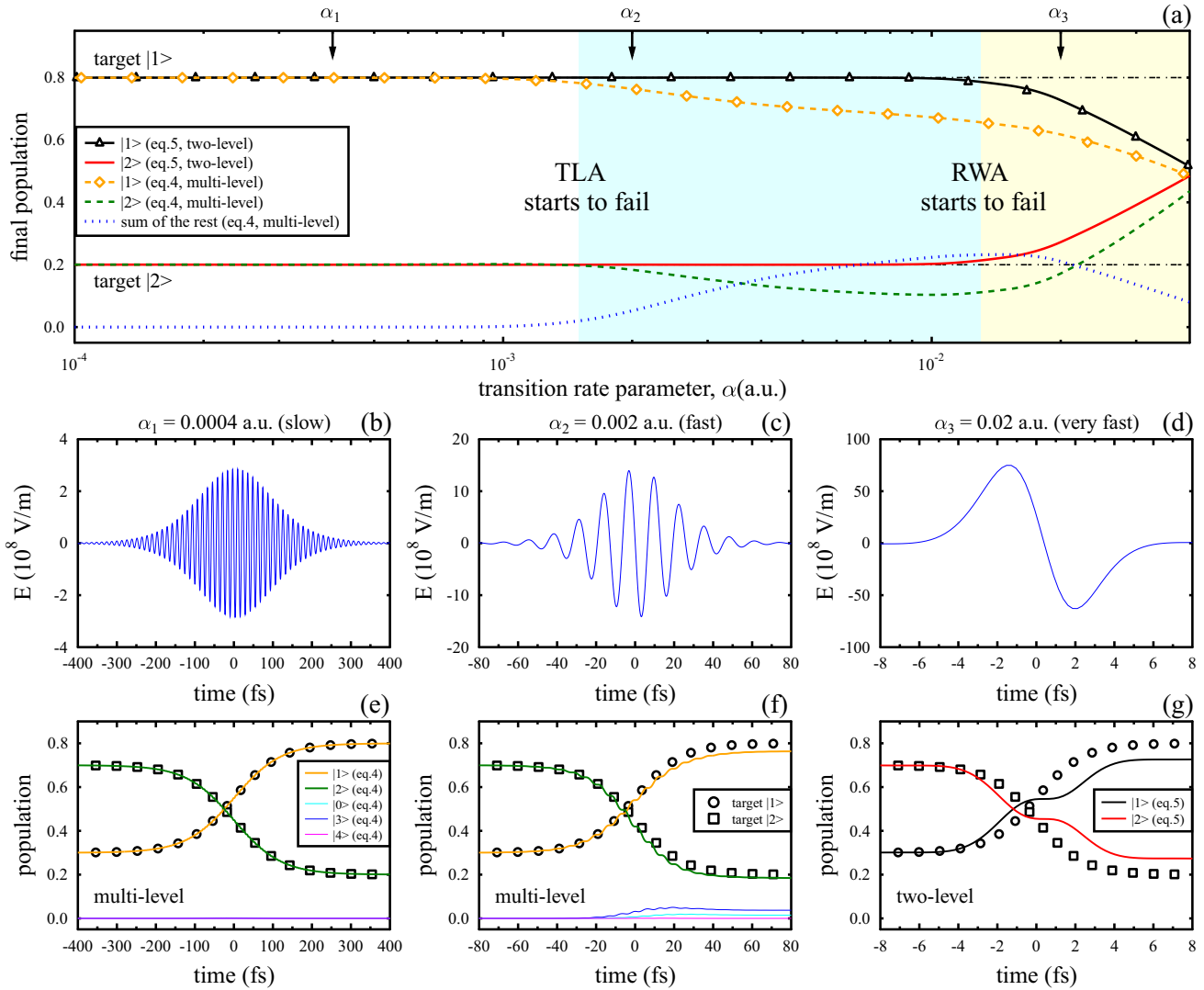
FIG. 2. Application of the $E(t)$ engineered laser pulse [Eq. (19)] to control the population dynamics of the $|1\rangle \rightarrow |2\rangle$ transition in HeH$^+$. A wide range of the α transition parameter is considered (a) to achieve a complete control over the rate of transition and the final target $|1\rangle$ and $|2\rangle$ populations (dashed-dotted horizontal lines). The initial population ratio of $|1\rangle$ and $|2\rangle$ is 0.3:0.7 ($p^i = 0.3$), and the final target population distribution of these states is 0.8:0.2 ($p^f = 0.8$) [for the control function, see Eq. (18)]. Upon fast transitions, the two-level approximation is violated as other states get populated, and we only approximately reach the target superposition (f). On the other hand, applying sufficiently slow transitions, any desired population dynamics is achieved with $E(t)$ (see the perfect matching of the control functions and the numerically obtained populations in e). Very fast transitions violate not only the TLA but the RWA (g). The full results are calculated in the space of 10 vibrational states with the TDEC method [Eq. (4)], while Eq. (5) is solved to obtain the TLA populations without the RWA.

required transitions are very fast, the field becomes single-cycle, very strong and short [Fig. 2(d) [87]] and the RWA starts to fail [light yellow area in Fig. 2(a)]. Owing to the breakdown of the RWA, the molecule can only approximately follow the prescribed path [Fig. 2(g)].

To demonstrate the wide range of applications provided by our engineered pulse [Eq. (17)], let us consider an oscillatory behavior of the population dynamics. Rabi oscillations are ubiquitous in physics with applications in different areas. They were found to play an important role, e.g., in vibronic transitions of diatomic molecules [88,89], and thus they are expected to have clear fingerprints in the energy spectrum of the particles emitted during the break-up of molecules. To induce an arbitrary number of Rabi oscillations between the

controlled vibrational states $|1\rangle$ and $|2\rangle$, the following control function is introduced:

$$\eta(t) = p^i + \frac{1}{2}\left[1 + \tanh\left(t + \frac{\tau}{2}\right)\right]A\sin^2\left(n\frac{\pi t}{\tau} + n\frac{\pi}{2}\right)$$
$$\times \frac{1}{2}\left[1 - \tanh\left(t - \frac{\tau}{2}\right)\right]. \quad (20)$$

In Eq. (20), $p^i = |a_1(t = -\infty)|^2$ is the initial population of $|1\rangle$ as before, and n is a positive integer that controls the number of Rabi cycles to be completed by the system in the time interval $[-\frac{\tau}{2}, \frac{\tau}{2}]$. Applying the above control function in Eq. (17), the population of $|1\rangle$ is expected to oscillate between p^i and $p^i + A$, meanwhile that of $|2\rangle$ is dictated by the norm conservation rule. The results concerning the controlled Rabi
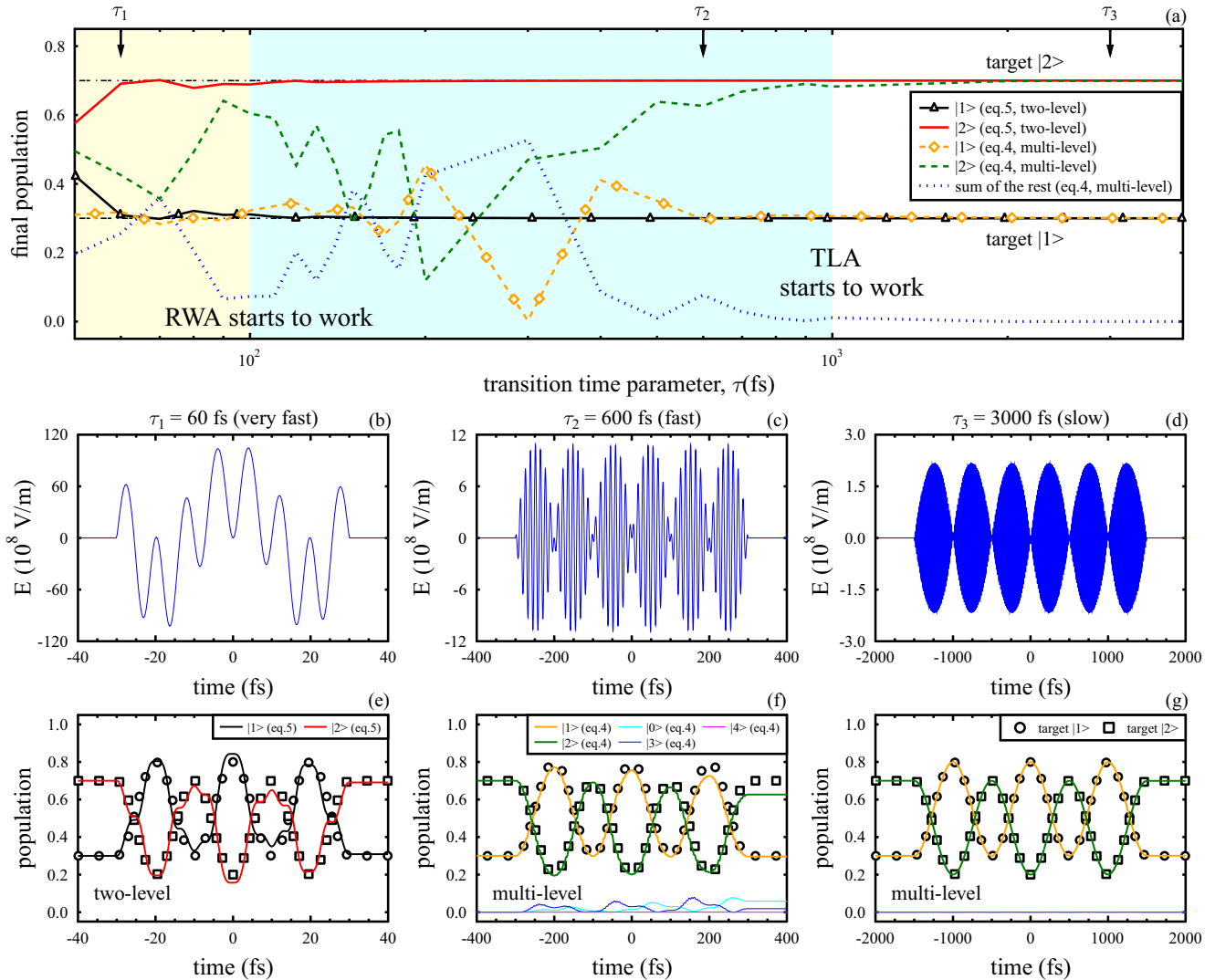
FIG. 3. Application of the $E(t)$ engineered laser pulse [Eq. (17)] to control the population dynamics of the $|1\rangle \leftrightarrow |2\rangle$ Rabi oscillations in HeH$^+$. A wide range of the τ transition time parameter is considered (a) to achieve a complete control over the rate of transition and the final target $|1\rangle$ and $|2\rangle$ populations (dashed-dotted horizontal lines). The initial population ratio of $|1\rangle$ and $|2\rangle$ is 0.3:0.7 ($p^i = 0.3$), the amplitude of population oscillation is $A = 0.5$, and the desired number of Rabi cycles is $n = 3$ [for the control function, see Eq. (20)]. Upon fast transitions, the two-level approximation is violated as other states get populated, and we only approximately reach the target path (f). On the other hand, applying sufficiently slow transitions, any desired population dynamics is achieved with $E(t)$ (see the perfect matching of the control functions and the numerically obtained populations in g). Very fast transitions violate not only the TLA but also the RWA (e). The full results are calculated in the space of 10 vibrational states with the TDEC method [Eq. (4)], while Eq. (5) is solved to obtain the TLA populations without the RWA.

dynamics of HeH$^+$ are presented in Fig. 3. Here the same initial condition is applied as in Fig. 2 ($p^i = 0.3$). According to Eq. (20), the molecule is required to complete $n = 3$ Rabi cycles with a population amplitude of $A = 0.5$. The time of transition is dictated by the τ parameter, which is varied to find the optimal control pulse shapes [see Fig. 3(a)]. Similarly to the case of smooth transitions (Fig. 2), if the desired Rabi-like transition is very fast ($\tau < 100$ fs) the RWA + AE fail and the numerical populations cannot follow exactly the target values [yellow area in Fig. 3(a)]. As the transition time is increased ($\tau > 100$ fs) the RWA starts to work as shown by the agreement of the two-level populations (solid red and black lines) and the target populations (horizontal dashed-dotted lines) in the light blue area of Fig. 3(a). In this

transition time interval (100 fs $< \tau <$ 1000 fs) the AE is not working yet as revealed by the disagreement of the accurate multilevel (TDEC) populations and the target populations. The population of the close-lying states is significant in this region [dotted line in Fig. 3(a)], and it becomes negligible only when $\tau > 1000$ fs, indicating that there not only the RWA but also the AE and thus the TLA starts to work. As a result, the molecule perfectly follows the predefined path even when it features several oscillations [Fig. 3(g)].

Regarding the validity conditions for the presented control, one can conclude from Figs. 2 and 3 that, the fulfillment of the AE imposes a stricter condition on the engineered laser pulse than the fulfillment of the RWA. In other words, satisfying merely the RWA does not guarantee a proper operation of
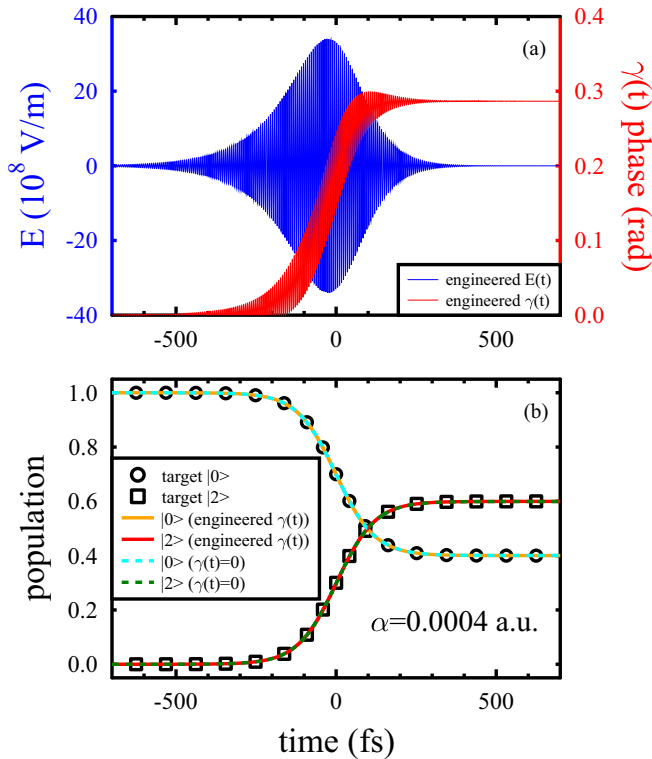
FIG. 4. Control of the $|0\rangle \rightarrow |2\rangle$ transition of HeH$^+$, using $E(t)$ in Eq. (19) either with engineered $\gamma(t)$ or with $\gamma(t) = 0$. Due to the multicycle character of the control field (a), the system is driven along the user-defined quantum path (open symbols in b) not only when $\gamma(t)$ is engineered in an iterative manner (and hence the time-dependent resonance condition is fulfilled at each moment of time), but also when $\gamma(t) = 0$ is applied. As the dynamically shifted molecular levels follow the rapidly oscillating electric field [Eq. (8)], the impact of the nuclear permanent dipoles μ_{kk} is washed out when the laser pulse supports many cycles, and as a consequence, population is transferred efficiently even when the time-dependent resonance condition is not fulfilled accurately ($\gamma(t) = 0$). The applied control parameters are $p^i = 1.0$, $p^f = 0.4$, and $\alpha = 0.0004$ a.u. The presented results are calculated in the space of 10 vibrational states with the TDEC method [Eq. (4)].

the control scheme when it is applied to a realistic multilevel system. One has to make sure that the pulse bandwidth is narrow enough to avoid overlapping with unwanted close-lying states and hence to make the AE work. This is done by increasing the pulse duration beyond the value required by the RWA. Comparing the above-discussed two kinds of system dynamics, namely the smooth transitions (Fig. 2) and the Rabi oscillations (Fig. 3), it is seen that much longer pulses are required for the scheme to work properly in the case when the desired dynamics get complicated. Contrary to smooth transitions, if the system undergoes several oscillations the RWA + AE have to be satisfied for each half-Rabi cycle which makes the control procedure slower.

As the nuclear dipole matrix μ_{jk} is a full matrix [84], the transition between any pair of states can be controlled by an appropriately shaped $E(t)$. This is demonstrated in Fig. 4, where the $|0\rangle \rightarrow |2\rangle$ transition of HeH$^+$ is considered. As the magnitude of the transition dipole for the $|0\rangle \rightarrow |2\rangle$

transition is almost nine times smaller than for $|1\rangle \rightarrow |2\rangle$, the required electric field strength is now significantly higher then before (e.g., in Fig. 2). The optimal shape of $E(t)$ for driving HeH$^+$ from a 1:0 initial population distribution of the $|0\rangle$ and $|2\rangle$ states, respectively to a final population ratio 0.4:0.6, is shown in Fig. 4(a) by the solid blue line. For completeness, the engineered $\gamma(t)$ phase of the field is also shown by the solid red line. Despite the increased field strength, the molecule is efficiently driven along the predefined path even when the controlled states are remotely coupled [see the perfect agreement of the solid lines and open symbols in Fig. 4(b)]. Importantly, the molecule also follows the target path when $\gamma(t) = 0$ is applied [dashed lines in Fig. 4(b)]. The agreement of the system dynamics driven with $\gamma(t) \neq 0$ and $\gamma(t) = 0$ may not hold for single-cycle pulses, but as we saw in Figs. 2 and 3, for a proper operation of the presented control, $E(t)$ has to support many cycles. In such a case (see, e.g., Fig. 4), the controlled molecular levels rapidly oscillate via the nuclear permanent dipoles μ_{kk} [see Eq. (8)]. According to Fig. 4(b), the molecule cannot follow the fast oscillations and the impact of the permanent dipoles is washed out in high frequency multicycle laser fields. As a result, population if efficiently transferred even when the time-dependent resonance condition is not fulfilled at each moment of time, i.e., when $\gamma(t) = 0$.

Further studying the applicability of the presented control, let us now inspect how sensitive $E(t)$ is to the imperfections of its parameters. As it was revealed in Fig. 4, $E(t)$ is very robust against variations in the $\gamma(t)$ field phase. Therefore we focus on the remaining system specific parameters, like the Ω Rabi frequency and the ω_{res} resonance angular frequency. The imperfections of these quantites are defined by the following relations:

$$\Omega' = (1 + \delta_\Omega)\Omega, \tag{21a}$$

$$\omega'_{\text{res}} = (1 + \delta_\omega)\omega_{\text{res}}. \tag{21b}$$

Varying the δ_Ω and δ_ω parameters in Eqs. (21a) and (21b), one can simulate possible preparation errors occurring in an experimental realization of $E(t)$. The obtained results are shown in Fig. 5 for the the control of the $|1\rangle \rightarrow |2\rangle$ transition using $p^i = 0.3$, $p^f = 0.8$ and $\alpha = 0.0004$ a.u. As seen in Fig. 5, the final target population of the $|1\rangle$ state (0.8, dashed line) is reached by $E(t)$ in a wide interval of the imperfection parameters. Deviation of the Rabi frequency from its optimal value ($\delta_\Omega = 0$) can be compensated by a proper positive or negative detuning of the control pulse (see the dashed line in Fig. 5). Interestingly this holds only when Ω is underestimated, namely when $\delta_\Omega < 0$. In such a case the peak value of $E(t)$ is larger than the optimal one dictated by Eq. (19) [see Eq. (7) for the relation between Ω and μ]. Detuning $E(t)$ from the (optimal) exact resonance either positively or negatively can compensate this unfavoured underestimation of Ω, and as a result the molecule is still driven to the desired final state. According to Fig. 5, $\pm 1\%$ detuning of ω_{res} is able to compensate ca. 15% error of the Ω Rabi frequency without the promotion of noticeable amount of population to the close-lying states.

As a final example, we would like to demonstrate how our control scheme can be applied to successively excite the
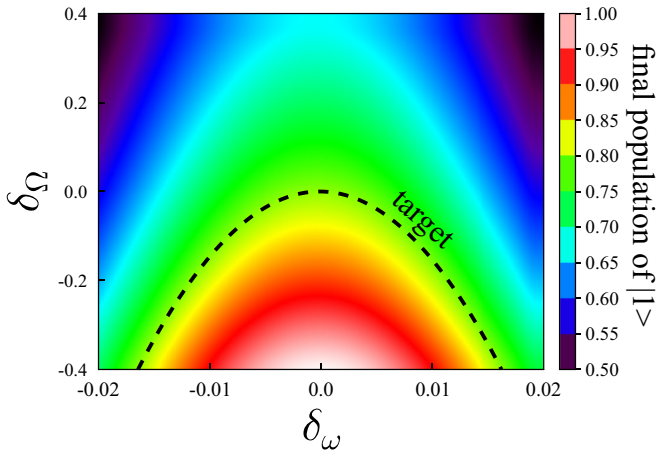
FIG. 5. Final population of the first excited vibrational state of HeH$^+$ as a function of the laser parameter imperfections defined in Eqs. (21a) and (21b). Deviations from the optimal values of the Rabi frequency and the resonance laser frequency lead to a deterioration of the final $|1\rangle$ state population from its target value of 0.8. A proper modification of the carrier laser frequency and the Rabi frequency can, however, still maintain the final target population (see the dashed line). The remaining fixed values of the applied laser pulses are $\alpha = 0.0004$ a.u., $p^i = 0.3$, and $p^f = 0.8$ [see also Fig. 2(b)]. The presented results are obtained by the TDEC method solving Eq. (4) in the space of 10 vibrational states, with $E(t)$ in Eq. (19).

FIG. 6. Vibrational ladder climbing of the HeH$^+$ molecule, applying either a single (a, b) or a double (c, d) step size. The applied laser pulse sequences are engineered such that a complete population inversion is induced between the successively coupled pairs of states $|j\rangle \rightarrow |k\rangle$ [for the individual $E(t)$ pulses of the pulse sequences, see Eq. (19)]. For each pulse, $p^i = 1$ and $p^f = 0$ are applied and the α transition rate parameter is chosen such that the TLA+RWA, and thus the control scheme, remain valid (3×10^{-4} a.u. $< \alpha < 7 \times 10^{-4}$ a.u.). The presented results are obtained by the TDWP method, setting the molecule initially in its vibrational ground state $|0\rangle$.

molecule from the vibrational ground state to high-lying vibrational states. Since the direct dissociation of HeH$^+$ from the vibrational ground state is very unlikely for the considered MIR photon energies [83], vibrational ladder climbing (VLC) can help enhancing the dissociation probability by bringing the molecule near the potential barrier where the bound-to-unbound transition dipole moments (TDM) are significantly larger. Owing to the anharmonicity of the ground-state potential, different photon energies are required for the consecutive vibrational excitations of the molecule [83]. As a consequence, we apply a sequence of nonoverlapping resonant laser pulses each of them with a different central angular frequency. The individual pulses are engineered according to Eq. (19) using $p^i = 1$ and $p^f = 0$ in order to induce a complete population inversion between the corresponding controlled pair of states. The obtained pulses of the sequence are π pulses (irrespective of α) with an appropriate frequency chirping, such that the emerging level shifts are compensated and population is transferred efficiently. The value of the α transition rate parameter is chosen to fulfill the validity condition for each transition. The simulated results of the vibrational ladder climbing of HeH$^+$ are shown in Fig. 6 both for a single [Figs. 6(a) and 6(b)] and a double step size [Figs. 6(c) and 6(d)], namely, when either first neighbor states or second neighbor states are coupled consecutively by the individual pulses. As the magnitude of the TDM between high-lying states is larger than between low-lying ones [84], the amplitudes of the individual engineered pulses exhibit a decreasing trend regardless of the step size [Figs. 6(a) and 6(c)]. As mentioned already, the second neighbor states are more weakly coupled than the first neighbor states, therefore ladder climbing via double step size requires stronger

pulses. Despite this, the molecule is still efficiently excited to the $|8\rangle$ state via second neighbor states using the present control scheme [gray line with dots in Fig. 6(d)]. Owing to the larger photon energies applied in the case of excitation via second neighbors, ladder climbing is completed much faster than in the case of single step size. The application of much larger step size may not reduce further the total duration of climbing. Since remotely coupled states are much more weakly coupled than first neighbor states, unwanted transitions to these direct neighbor states can reduce the efficiency of VLC. This can be resolved by reducing α, but the price is that the total duration of VLC will get longer in that case.

Reduction of the total duration of the process is important for instance for the ladder descending in the preparation of cold molecules [76]. Furthermore, in certain molecules the dipole coupling vanishes between neighbor states, and in such a case the application of increased step size is an efficient way of climbing the ladder [75]. Our method for VLC can be considered complementary to existing ones (for a detailed comparative study, see Ref. [76]). As it applies a nonoverlapping sequence of chirped π pulses, the total duration of climbing or descending is expected to be longer than in the case of one or two chirped pulses [75], but increasing the step size can further accelerate the process. While our method is rather robust against phase variations of the individual pulses, this may not be the case in other methods utilizing single chirped pulses, the frequency modulations of which are determined by different optimization techniques.

After bringing the molecule close to the dissociation threshold of the ground electronic state ($\nu = 8$), we now apply an intense ultrashort laser pulse to initiate the dissociation of HeH$^+$:

$$\mathcal{E}(t) = \mathcal{E}_0 e^{-\frac{t^2}{2T^2}} \cos(\omega_L t). \tag{22}$$

In Eq. (22) the T pulse duration parameter is related to the full width at half maximum (fwhm) as fwhm $= 2T\sqrt{ln2}$, while the $\mathcal{E}$ electric field strength value is linked to the laser intensity as $I = \mathcal{E}^2/8\pi\alpha_{fs}$ (here α_{fs} is the fine structure constant). The kinetic energy release (KER) spectra obtained for $\omega_L = 1$ eV and fwhm $= 20$ fs by Fourier transforming the outgoing wave packets (TDWP method [84]), are shown in Fig. 7(a) for increasing laser intensities. As expected in the weak-field limit, a single peak develops around the nominal position [$\omega_8 + \omega_L$, the middle vertical dashed line in Fig. 7(a)] which is followed by equally spaced higher order above-threshold dissociation (ATD) peaks, each of them shifted by the photon energy ω_L [78]. For clarity, these ATD peaks are not shown in Fig. 7 as they have significantly lower intensity, and we would like to focus here on the structural behavior of the primary dissociation peak. Upon increasing laser-molecule coupling, not only the dissociation probability (p_{diss}) increases significantly, but importantly the single dissociation peak is replaced by a distinct multipeak pattern. This happens when the depletion of the initial state is significant ($I > 10^{15}$ W/cm^2). To understand the physical origin of the emerging multipeak pattern in the spectrum, it is useful to inspect the population dynamics of the molecule. The time-dependent vibrational state populations shown in Fig. 7(b) reveal that enhanced Rabi oscillations are induced between the initial state (solid blue line) and the continuum (dotted red line). As a result of the consecutive back and forth population transfer, the molecule gradually dissociates, meanwhile other close-lying bound states also get involved in the dynamics. This is better illustrated in Fig. 7(c), where the population dynamics is shown in the vicinity of the maximum of the pulse ($t = 0$). Here one can see that besides the initially populated $\nu = 8$ state (blue line), the $\nu = 7$ (magenta line) and $\nu = 9$ (light green line) states also participate in the Rabi oscillations, though with a slightly lower probability than the $\nu = 8$ state. As a result, dissociation occurs from these levels too, which is reflected by the appearance of the side peaks around the main dissociation peak in Fig. 7(a). Due to the shift of the molecular levels in the intense laser field, the energetic position of the spectrum peaks do not match exactly the nominal peak positions indicated by the vertical dashed lines in Fig. 7(a). We note here that the higher order ATD peaks (not shown here) also exhibit the same kind of structural behavior. The distinct multipeak pattern found in the strong-field KER spectrum might be affected under very realistic conditions, e.g., when the ionization of HeH$^+$ is properly taken into account [80]. This is an intriguing subject which can be addressed in a separate work. Here we have carried out extended numerical simulations allowing the molecule to dynamically rotate, and found that the multipeak pattern remains observable in the KER spectrum even for rotating-vibrating molecules [84].

Finally a few words about the possible extensions of the presented control scheme. The proposed reverse
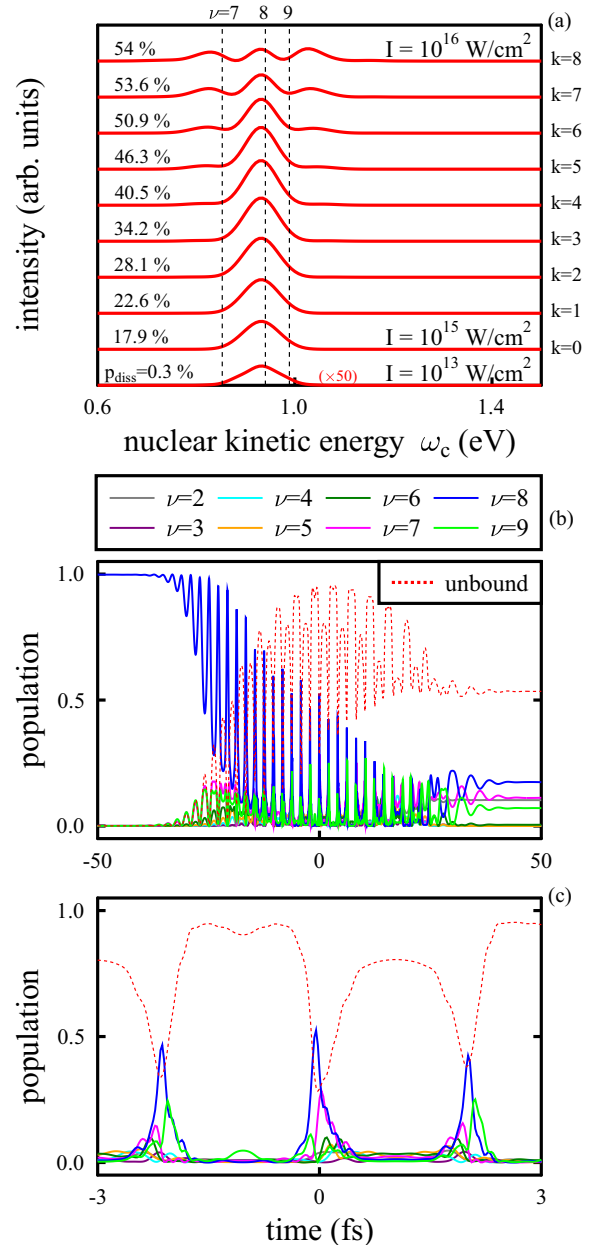
FIG. 7. Ground-state dissociation of the HeH$^+$ molecule induced by strong laser pulses of fwhm $= 20$ fs duration and $\omega_L = 1$ eV carrier frequency. The molecule is prepared initially in a high-lying vibrational state ($\nu = 8$) to allow for enhanced excitation beyond the potential barrier of the ground electronic state. (a) The KER spectra obtained by solving the TDSE for increasing laser intensities ($I_k = 10^{k/8} \times 10^{15}$ W/cm^2, $k = 0, 1, 2 \ldots, 8$) exhibit a pronounced multipeak pattern when the depletion of the initial state is large. The vertical dashed lines indicate the relevant vibrational eigenenergies shifted by the photon energy, $\omega_i + \omega_L$ ($i = 7, 8, 9$). (b) Time-dependent populations of the bound and unbound states for $I = 10^{7/8} \times 10^{15}$ W/cm^2. Owing to the Rabi oscillations between the initial and continuum states in the strong field, the molecule gradually dissociates. (c) Besides the initially populated $\nu = 8$ state (blue line), the neighboring $\nu = 7$ (magenta line) and $\nu = 9$ (light green line) states also participate in the Rabi dynamics and subsequent dissociation, giving rise to the multipeak pattern of the spectrum found in (a). The presented results are obtained by the TDWP method.

engineering was tailored to control weak and intermediate laser-molecule interactions, which are dominated by single-photon transitions. In the case of strong laser fields, the induced dipole moments have to be accounted properly as they can significantly modify the time-dependent molecular level shifts [36,90,91]. Incorporating polarizability effects in the presented reverse engineering via the nonessential states is possible as it has been demonstrated by us recently when studying strong-field atomic transitions [58]. The presented method is not limited to linearly polarized laser pulses. Elliptically polarized pulses can be considered as the sum of two perpendicular linearly polarized fields with different amplitudes and a phase difference of $\pi/2$ [92]. Such pulses can be transformed into the general form of Eq. (1), though with a different total phase. Elliptically polarized laser pulses may find important application in the case of rotating molecules. Extension of the present control to rotating-vibrating diatomic molecules requires the knowledge of many rovibrational eigenenergies and eigenstates as well as the corresponding dipole matrix elements [93]. Owing to the dense level spacing, the state-to-state control gets substantially slower as the validity conditions of the applied approximations can be satisfied with long pulses. Extending the proposed protocol for polyatomic molecules is even more challenging. For polyatomics, the dipole moment can have three components. Including rotation is crucial in that case, since the relative magnitude of different dipole components change with the orientation of the molecule. Although highly accurate full dimensional rotational-vibrational levels of polyatomics are available [25], the issue of degenerate energy levels can cause further difficulties.

V. CONCLUSIONS

The reverse engineering scheme presented in this paper allows for the design of analytical laser pulses to drive diatomic molecular transitions along user-defined pathways. The envelope and phase functions of the applied laser pulses have been engineered to distort the molecular potential via the electric permanent dipole function such that the aligned diatomic molecule follows a prescribed quantum path. This has been done by inversely solving a minimal two-level model that includes dynamical level shifts caused by the electric permanent dipole moment of the considered electronic state. The presented scheme has been validated by solving the full TDSE of the HeH^+ molecular ion accurately. We have shown that the fulfillment of the adiabatic elimination imposes a stricter condition than the fulfillment of the rotating wave approximation, meaning that the optimal pulse has to support many cycles for a proper operation of the scheme. The pulse design has been demonstrated by driving smooth and even oscillatory transitions between different eigenstates of the molecule. Using an appropriately shaped pulse sequence, the consecutive vibrational excitation of HeH^+ has been also illustrated with the aim to enhance the dissociation probability in the ground electronic state. Several possible extensions of the proposed control method has been also discussed. Within the scope of the applied approximations, the engineered laser pulse was found rather robust against imperfections of the different control parameters appearing in the expression of the laser pulse. In particular, the impact of the permanent dipoles was found marginal in rapidly oscillating fields.

[1] D. J. Tannor, *Molecules in Laser Fields*, edited by A. D. Bandrauk (Marcel Dekker, New York, 1994), pp. 403–446.

[2] S. A. Rice and M. Zhao, *Optical Control of Molecular Dynamics* (Wiley, New York, 2000).

[3] M. Shapiro and P. Brumer, *Principles of Quantum Control of Molecular Processes* (Wiley, New York, 2003).

[4] N. V. Vitanov, T. Halfmann, B. W. Shore, and K. Bergmann, Annu. Rev. Phys. Chem. **52**, 763 (2001).

[5] R. Kosloff, A. D. Hammerich, and D. J. Tannor, Phys. Rev. Lett. **69**, 2172 (1992).

[6] V. S. Malinovsky, C. Meier, and D. J. Tannor, Chem. Phys. **221**, 67 (1997).

[7] S. Gräfe, C. Meier, and V. Engel, J. Chem. Phys. **122**, 184103 (2005).

[8] D. Guéry-Odelin, A. Ruschhaupt, A. Kiely, E. Torrontegui, S. Martínez-Garaot, and J. G. Muga, Rev. Mod. Phys. **91**, 045001 (2019).

[9] D. Stefanatos and E. Paspalakis, Europhys. Lett. **132**, 60001 (2020).

[10] R. S. Judson and H. Rabitz, Phys. Rev. Lett. **68**, 1500 (1992).

[11] T. C. Weinacht and P. H. Bucksbaum, J. Opt. B: Quantum Semiclass. Opt. **4**, R35 (2002).

[12] W. Zhu, J. Botina, and H. Rabitz, J. Chem. Phys. **108**, 1953 (1998).

[13] P. Kumar, S. Sharma, and H. Singh, J. Theor. Comput. Chem. **8**, 157 (2009).

[14] P. Kumar, S. A. Malinovskaya, and V. S. Malinovsky, Phys. Rev. A **90**, 033427 (2014).

[15] P. V. D. Hoff, S. Thallmair, M. Kowalewski, R. Siemering, and R. D. Vivie-Riedle, Phys. Chem. Chem. Phys. **14**, 14460 (2012).

[16] G. A. Worth and G. W. Richings, Annu. Rep. Prog. Chem. C **109**, 113 (2013).

[17] N. V. Golubev, V. Despré, and A. I. Kuleff, J. Mod. Opt. **64**, 1031 (2017).

[18] I. R. Solá, B. Y. Chang, S. A. Malinovskaya, and V. S. Malinovsky, Adv. At. Mol. Opt. Phys. **67**, 151 (2018).

[19] S. Zou, Q. Ren, G. G. Balint-Kurti, and F. R. Manby, Phys. Rev. Lett. **96**, 243003 (2006).

[20] S. Zou, C. Sanz, and G. G. Balint-Kurti, J. Chem. Phys. **129**, 124307 (2008).

[21] Q. Zhang, X. Chen, and D. Guéry-Odelin, Sci. Rep. **7**, 15814 (2017).

[22] S. Ibáñez, Y.-C. Li, X. Chen, and J. G. Muga, Phys. Rev. A **92**, 062136 (2015).

[23] S. Xiao, Q. Ke, and Y. Ji, Can. J. Phys. **100**, 371 (2022).

[24] J. Hu, Q. Ke, and Y. Ji, Int. J. Mod. Phys. B **36**, 2250013 (2022).

[25] C. Fábri, R. Marquardt, A. G. Császár, and M. Quack, J. Chem. Phys. **150**, 014102 (2019).

[26] M. Heindl and L. González, J. Phys. Chem. Lett. **13**, 1894 (2022).

[27] M. Sala, M. Saab, B. Lasorne, F. Gatti, and S. Guérin, J. Chem. Phys. **140**, 194309 (2014).

[28] S. Mainali, F. Gatti, and O. Atabek, Chinese Opt. Lett. **20**, 100007 (2022).

[29] B. J. Sussman, D. Townsend, M. Y. Ivanov, and A. Stolow, Science **314**, 278 (2006).

[30] B. J. Sussman, Am. J. Phys. **79**, 477 (2011).

[31] J.-C. Liu, C.-K. Wang, and F. Gel'mukhanov, Phys. Rev. A **76**, 043422 (2007).

[32] G. A. Worth and C. Sanz-Sanz, Phys. Chem. Chem. Phys. **12**, 15570 (2010).

[33] C. Sanz-Sanz, G. W. Richings, and G. A. Worth, Faraday Discuss. **153**, 275 (2011).

[34] D. Geißler, P. Marquetand, J. González-Vázquez, L. González, T. Rozgonyi, and T. Weinacht, J. Phys. Chem. A **116**, 11434 (2012).

[35] S. Scheit, Y. Arasaki, and K. Takatsuka, J. Phys. Chem. A **116**, 2644 (2012).

[36] I. R. Solá, J. González-Vázquez, R. de Nalda, and L. Bañares, Phys. Chem. Chem. Phys. **17**, 13183 (2015).

[37] C.-C. Shu, E. F. Thomas, and N. E. Henriksen, Chem. Phys. Lett. **683**, 234 (2017).

[38] D. Dey and N. E. Henriksen, J. Chem. Phys. **148**, 234307 (2018).

[39] A. Tóth, A. Csehi, G. J. Halász, and Á. Vibók, Phys. Rev. Res. **2**, 013338 (2020).

[40] L. Biró and A. Csehi, Phys. Chem. Chem. Phys. **24**, 13234 (2022).

[41] B. Mignolet, B. F. E. Curchod, F. Remacle, and T. J. Martínez, J. Phys. Chem. Lett. **10**, 742 (2019).

[42] N. Moiseyev, M. Šindelka, and L. S. Cederbaum, J. Phys. B: At. Mol. Opt. Phys. **41**, 221001 (2008).

[43] G. J. Halász, Á. Vibók, and L. S. Cederbaum, J. Phys. Chem. Lett. **6**, 348 (2015).

[44] A. Csehi, G. J. Halász, L. S. Cederbaum, and Á. Vibók, J. Phys. Chem. Lett. **8**, 1624 (2017).

[45] G. J. Halász, M. Šindelka, N. Moiseyev, L. S. Cederbaum, and Á. Vibók, J. Phys. Chem. A **116**, 2636 (2012).

[46] P. Badankó, G. J. Halász, L. S. Cederbaum, Á. Vibók, and A. Csehi, J. Chem. Phys. **149**, 181101 (2018).

[47] T. Szidarovszky, A. G. Császár, G. J. Halász, and Á. Vibók, Phys. Rev. A **100**, 033414 (2019).

[48] C. Fábri, G. J. Halász, and Á. Vibók, J. Phys. Chem. Lett. **13**, 1172 (2022).

[49] A. Natan, M. R. Ware, V. S. Prabhudesai, U. Lev, B. D. Bruner, O. Heber, and P. H. Bucksbaum, Phys. Rev. Lett. **116**, 143004 (2016).

[50] M. E. Corrales, J. González-Vázquez, G. Balerdi, I. R. Solá, R. de Nalda, and L. Bañares, Nat. Chem. **6**, 785 (2014).

[51] M. Kübel, M. Spanner, Z. Dube, A. Y. Naumov, S. Chelkowski, A. D. Bandrauk, M. J. Vrakking, P. B. Corkum, D. Villeneuve, and A. Staudte, Nat. Commun. **11**, 2596 (2020).

[52] N. V. Golubev and A. I. Kuleff, Phys. Rev. A **90**, 035401 (2014).

[53] N. V. Golubev and A. I. Kuleff, Phys. Rev. A **91**, 051401 (2015).

[54] I. Medina and F. L. Semião, Phys. Rev. A **100**, 012103 (2019).

[55] A. Csehi, J. Phys. B: At. Mol. Opt. Phys. **52**, 195004 (2019).

[56] D. Ran, W.-J. Shan, Z.-C. Shi, Z.-B. Yang, J. Song, and Y. Xia, Phys. Rev. A **101**, 023822 (2020).

[57] D. Ran, B. Zhang, Y.-H. Chen, Z.-C. Shi, Y. Xia, R. Ianconescu, J. Scheuer, and A. Gover, Opt. Lett. **45**, 3597 (2020).

[58] A. Tóth and A. Csehi, Phys. Rev. A **104**, 063102 (2021).

[59] T. H. Einwohner, J. Wong, and J. C. Garrison, Phys. Rev. A **14**, 1452 (1976).

[60] M. A. Kmetic and W. J. Meath, Phys. Lett. A **108**, 340 (1985).

[61] A. E. Kondo, V. M. Blokker, and W. J. Meath, J. Chem. Phys. **96**, 2544 (1992).

[62] A. Brown, W. J. Meath, and P. Tran, Phys. Rev. A **63**, 013403 (2000).

[63] L. Biró and A. Csehi, J. Mod. Opt. **66**, 119 (2019).

[64] B. Kaufman, T. Rozgonyi, P. Marquetand, and T. C. Weinacht, Phys. Rev. A **102**, 063117 (2020).

[65] A. Kiely and A. Ruschhaupt, J. Phys. B: At. Mol. Opt. Phys. **47**, 115501 (2014).

[66] S. Chelkowski, A. D. Bandrauk, and P. B. Corkum, Phys. Rev. Lett. **65**, 2355 (1990).

[67] D. J. Maas, D. I. Duncan, R. B. Vrijen, W. J. van der Zande, and L. D. Noordam, Chem. Phys. Lett. **290**, 75 (1998).

[68] T. Witte, T. Hornung, L. Windhorn, D. Proch, R. de Vivie-Riedle, M. Motzkus, and K. L. Kompa, J. Chem. Phys. **118**, 2021 (2003).

[69] C. Ventalon, J. M. Fraser, M. H. Vos, A. Alexandrou, J.-L. Martin, and M. Joffre, Proc. Natl. Acad. Sci. USA **101**, 13216 (2004).

[70] G. Marcus, A. Zigler, and L. Friedland, Europhys. Lett. **74**, 43 (2006).

[71] C. Falvo, A. Debnath, and C. Meier, J. Chem. Phys. **138**, 145101 (2013).

[72] J. P. Kraack and P. Hamm, Phys. Chem. Chem. Phys. **18**, 16088 (2016).

[73] H. Daoud, L. Joubert-Doriol, A. F. Izmaylov, and R. J. Dwayne Miller, Chem. Phys. **515**, 28 (2018).

[74] I. Morichika, K. Murata, A. Sakurai, K. Ishii, and S. Ashihara, Nat. Commun. **10**, 3893 (2019).

[75] T. Horiba, S. Shirai, and H. Hirai, Phys. Rev. A **105**, 013117 (2022).

[76] A. Devolder, M. Desouter-Lecomte, O. Atabek, E. Luc-Koenig, and O. Dulieu, Phys. Rev. A **103**, 033301 (2021).

[77] P. Tran, Phys. Rev. A **59**, 1444 (1999).

[78] D. Ursrey, F. Anis, and B. D. Esry, Phys. Rev. A **85**, 023429 (2012).

[79] D. Ursrey and B. D. Esry, Phys. Rev. A **96**, 063409 (2017).

[80] P. Wustelt, F. Oppermann, L. Yue, M. Möller, T. Stöhlker, M. Lein, S. Gräfe, G. G. Paulus, and A. M. Sayler, Phys. Rev. Lett. **121**, 073203 (2018).

[81] P. Wustelt, M. Kübel, G. G. Paulus, and A. M. Sayler, Adv. At. Mol. Opt. Phys. **69**, 67 (2020).

[82] F. Oppermann, P. Wustelt, T. Florin, S. Mhatre, S. Gräfe, G. G. Paulus, and M. Lein, J. Phys. B **53**, 174001 (2020).

[83] P. Wustelt, F. Oppermann, S. Mhatre, M. Kübel, A. M. Sayler, M. Lein, S. Gräfe, and G. G. Paulus, Phys. Rev. Lett. **127**, 043202 (2021).

[84] See Supplemental Material at http://link.aps.org/supplemental/10.1103/PhysRevA.106.043113 for material including (1) the nuclear dipole matrix in the ground electronic state of HeH$^+$, (2) the description of the TDEC and TDWP methods, (3) the impact of molecular rotation on the presented control scheme, and (4) information on the strong-field KER spectra.

[85] D. Tannor, *Introduction to Quantum Mechanics: A Time-Dependent Perspective* (University Science Books, Herndon, VA, 2005).

[86] C. Trallero-Herrero, J. L. Cohen, and T. C. Weinacht, Phys. Rev. Lett. **96**, 063603 (2006).

[87] For large α the zero integral of $E(t)$ is fulfilled only approximately, but in the region of operation (small α) this condition is automatically fulfilled due to the multicycle character of $E(t)$. Incorporating such a constraint into the presented reverse engineering is feasible.

[88] A. Palacios, H. Bachau, and F. Martín, Phys. Rev. A **74**, 031402 (2006).

[89] S. Wang, E. Lötstedt, J. Cao, Y. Fu, H. Zang, H. Li, T. Ando, A. Iwasaki, K. Yamanouchi, and H. Xu, Phys. Rev. A **104**, 032823 (2021).

[90] B. Y. Chang, I. R. Solá, and S. Shin, Int. J. Quantum Chem. **116**, 608 (2016).

[91] L. Yue, P. Wustelt, A. M. Sayler, F. Oppermann, M. Lein, G. G. Paulus, and S. Gräfe, Phys. Rev. A **98**, 043418 (2018).

[92] S. Carrasco, J. Rogan, J. A. Valdivia, B. Y. Chang, V. S. Malinovsky, and I. R. Solá, Phys. Chem. Chem. Phys. **24**, 2966 (2022).

[93] S. Hervé, F. L. Quéré, and R. Marquardt, J. Chem. Phys. **114**, 826 (2001); **116**, 3300 (2002); Int. J. Quantum Chem. **99**, 439 (2004).